NeuroImage 62 (2012) 1415–1428

Contents lists available at SciVerse ScienceDirect

NeuroImage

journal homepage: www.elsevier.com/locate/ynimg

Go with the flow: Use of a directed phase lag index (dPLI) to characterize patterns of phase relations in a large-scale model of brain dynamics

C.J. Stam, E.C.W. van Straaten *

Department of Clinical Neurophysiology, VU University Medical Center, P.O Box: 7057, 1007 MB Amsterdam, The Netherlands

ARTICLE INFO

Article history:
Accepted 19 May 2012
Available online 24 May 2012

Keywords:
Directed phase lag index
Effective connectivity
Modeling
Synchronization
Graph theory
Resting-state

ABSTRACT

We introduce a directed phase lag index to investigate the spatial and temporal pattern of phase relations of oscillatory activity in a model of macroscopic structural and functional brain networks. Direction of information flow was determined with the directed phase lag index (dPLI) defined as the probability that the instantaneous phase of X was smaller than the phase of Y (modulo π). X was said to phase-lead Y if $0.5 < dPLI_{XY} <= 1$. The dPLI was used to characterize the phase relations between simulated EEG time series. The model consisted of 78 brain regions, coupled according to DTI findings in human subjects (Gong et al., 2009). Activity of each brain region was simulated with a neural mass model. Phase patterns were investigated as a function of coupling strength without stimulation, and with stimulation of the primary visual areas. At rest a clear spatial pattern of phase relations emerged with regions belonging to the anterior part of the default mode network leading in phase and regions belonging to the posterior part of the default mode network and surrounding visual areas lagging in phase. Patterns of phase leading and lagging displayed characteristic patterns with time scales from a few hundred milliseconds to 1–2 s. Stimulation of the primary visual areas induced a reversal of the global phase pattern with the visual and basal temporal areas leading and the anterior and superior frontal areas lagging in phase. This study shows that the directed phase lag index (dPLI) is an effective measure to characterize spatial temporal patterns of phase relations at rest and during stimulation. Coupling strength and node degree were found to be critical determinants of the direction of information flow. At a timescale of milliseconds to seconds the phase dynamics revealed spontaneous structure that might correspond to previously described "microstates". Stimulation of two visual areas reversed the global pattern of phase relations.

Introduction

The focus in neuroscientific research is shifting from studies of local activation toward investigations of interactions and communication in brain networks from the neuronal level up to the macroscopic domain (Stam and van Straaten, 2012). There is increasing agreement that a proper understanding of normal brain function as well as its breakdown in various neurological and psychiatric disorders requires a complex network perspective of the brain (Bassett and Bullmore, 2009). The network approach to the brain has been stimulated by advances in technology such as high density EEG, MEG and structural and functional MRI, advances in signal processing, allowing reliable estimation of functional and effective connectivity, and perhaps most of all by the use of the mathematical framework of graph theory to understand the significance of organizational patterns in brain networks (Bullmore and Sporns, 2009; Stam and Reijneveld, 2007; van den Heuvel and Hulshoff Pol, 2010). As discussed in these reviews several studies have shown that the healthy brain can be described as a small-world network, combining dense local clustering with short average path lengths. In addition, brain networks show an approximately scale-free distribution of connections with a connectivity backbone of highly connected hubs regions in the default mode network. Furthermore, brain networks display a tendency of highly connected nodes to a hierarchical modular structure. These topological features of brain networks evolve in a systematic way during development, are under strong genetic control, and correlate consistently with measures of cognitive performance (Stam, 2010). Characteristic patterns of brain network "disorganization" have now been demonstrated in various disorders including Alzheimer's disease, schizophrenia and epilepsy (Kramer and Cash, 2012; Rubinov and Bassett, 2011; Xie and He, 2011).

Further progress in complex brain network studies will depend upon the development of more effective measures of connectivity and network topology, a more comprehensive view of the significance of empirical observations and ultimately the development of a general theory of brain networks. Development of models of brain networks in the context of computational neuroscience can play an important role in addressing these problems (Coombes, 2010; Deco et al., 2008, 2011; Suffczynski et al., 2006). The models of random, small-world and scale-free networks that initially inspired a graph theoretical approach to brain network studies are simple and mathematically

* Corresponding author. Fax: +31 20 4444816.
E-mail addresses: CJ.Stam@VUmc.nl (C.J. Stam), i.vanstraaten@VUmc.nl (E.C.W. van Straaten).

1053-8119/$ – see front matter © 2012 Elsevier Inc. All rights reserved.
doi:10.1016/j.neuroimage.2012.05.050

elegant, but lack adequate detail to explain all observations, and do not fit within a single framework (Stam and van Straaten, 2012). For instance, the small-world model cannot explain scale-free degree distributions and the presence of hubs, while the scale-free model cannot explain clustering. None of the basic models can explain hierarchical modularity and assortative mixing. In this respect computational models of small networks of interconnected neurons have been more successful. Models at the neuronal level have suggested possible scenarios for the emergence of small-world features, scale-free properties and modular structure (Rubinov et al., 2009; Siri et al., 2007; Wang et al., 2011). However, most observations in humans are at the level of macroscopic level of EEG, MEG and MRI.

Several studies have modeled the brain at the macroscopic level of interconnected neural masses. Typically, a neural mass describes the average activity of large numbers of interconnected excitatory and inhibitory neurons, producing an EEG-like signal that can be converted to a BOLD signal by a proper convolution. Structural connectivity between regions is often based upon available neuroanatomical data of monkey, cat or human brain networks. Honey et al. have shown that many features of functional brain networks can be reproduced in such models (Honey et al., 2007, 2009). The topology of functional brain networks was shown to be related to the topology of the underlying structural networks. Importantly, the topological patterns of functional networks depended upon the time scale of observation (Honey et al., 2007). The complex relation between structural and functional topology was confirmed in a simulation study by Ponten et al. (2010). In another study based upon the same model emergence of modular structure could be explained by the interaction between the influence of distance and synchronization on connection strength (Stam et al., 2010). Macroscopic studies of brain networks have also revealed the impact of local structural brain lesions on network architecture (Alstott et al., 2009; Honey and Sporns, 2008; Kaiser et al., 2007; Stam et al., 2010).

Macroscopic models of brain networks have often assumed bidirectional and symmetric interactions between brain regions. In contrast, in empirical studies there is increasing interest in asymmetric and causal interactions between brain regions (Stephan and Roebroeck, 2012). Previous studies have reported an anterior to posterior flow of gamma and delta activity (Llinás and Ribary, 1993; Massimini et al., 2004). An interesting question is whether macroscopic brain networks in a resting state can be expected to display a consistent pattern of asymmetric, possibly causal interactions. According to a proposal by Fries communication between brain regions may depend upon the existence of small, but consistent phase delays (Fries, 2005). Detection of these consistent but small phase delays might be difficult with the commonly used Granger-based approaches (Gourévitch et al., 2006). Measures that are based upon the statistics of phase differences between signals such as phase coherence, imaginary coherence, and the phase lag index do not take into account asymmetric relations but can be modified for this purpose. A measure of consistent phase differences between time series could be used to investigate whether the brain at rest displays a structured pattern of phase differences such as suggested by Llinás and Ribary (1993) and Massimini et al. (2004) and whether this pattern changes in a logical way after stimulation of selected brain regions.

In the present study we examined the presence and organization of patterns of phase differences between simulated EEG time series in a macroscopic brain model. EEG time series were simulated by neural mass models connected according to structural data of neuroanatomical brain networks described by Gong et al. (2009). To assess both the strength as well as the direction of phase relations between simulated EEG signals we introduce a directed phase lag index (dPLI) that is defined as the probability that the phase of one time series is smaller (modulo π) than the instantaneous phase of another signal. The topological patterns of dPLI were examined at different levels of global coupling strength in a resting-state as well as during simulated photic stimulation of the primary visual areas.

Methods

Phase lag index (PLI)

The phase lag index (PLI) is a measure of phase synchronization that is not sensitive to volume conduction or common reference effects (Stam et al., 2007). Since zero-lag synchronization is left out of the analysis, the reported coupling between time series is not based on common sources. The measure is based upon the concept of phase synchronization (for chaotic oscillators) as introduced by Rosenblum et al. (1996). If Φ_1 and Φ_2 are the phases of two time series, and Φ is the phase difference or relative phase, n to m (with n and m some integers) phase synchronization is defined as follows:

$$\left|\varphi_{n,m}\right| = |n\varphi_1 - m\varphi_2| < const \tag{1}$$

In the rest of this paper we restrict ourselves to the case of $n = m = 1$. To compute the phase synchronization it is necessary to know the instantaneous phase of the two signals involved. This can be done with the analytical signal concept and the Hilbert Transform (the approach with wavelets gives similar results: Burns, 2004). The analytical signal $\Psi(t)$ is complex with $s(t)$ a real time series and $\tilde{s}(t)$ the Hilbert transform of this real signal:

$$\psi(t) = s(t) + i\tilde{s}(t) = A(t)e^{i\varphi(t)} \tag{2}$$

The Hilbert transform of $s(t)$ is obtained as follows:

$$\tilde{s}(t) = \pi^{-1} P.V. \int_{-\infty}^{\infty} \frac{s(\tau)}{t-\tau} d\tau \tag{3}$$

Here P.V. refers to the Cauchy principle value. The Hilbert transform is related to the original signal by a phase shift of ½ π in the frequency domain without a change in the power spectrum. (The Hilbert transform can be computed by performing an FFT, shifting all the phases by ½ π, followed by an inverse FFT). From Eq. (2) both the instantaneous amplitude and the instantaneous phase can be computed. The phase $\Phi(t)$ at time t is given by:

$$\Phi(t) = \arctan \frac{\tilde{s}(t)}{s(t)} \tag{4}$$

Following Eq. (1) from the instantaneous phase of two signals the phase difference or relative phase is computed for each time sample. For the sake of simplicity in the following text $\Phi(t)$ refers to this phase difference between two signals. Different methods exist to determine whether this phase difference is bounded.

The idea behind the Phase Lag Index (PLI) is to make the estimation of phase synchronization less sensitive to the influence of common sources (volume conduction and/or active reference electrodes in the case of EEG) by quantifying the asymmetry of the distribution of phase differences, where the distribution is centered around a phase difference of zero. When no phase coupling exists between two time series this distribution is expected to be flat. Any deviation from this flat distribution is an indication of phase synchronization. Asymmetry of the phase difference distribution means that the likelihood that the phase difference Φ will be in the interval $-\pi < \Phi < 0$ is different from the likelihood that it will be in the interval $0 < \Phi < \pi$. This asymmetry indicates that there is a consistent, non zero phase difference ('lag') between the two time series; the existence of such a phase difference or time lag cannot be explained by the influence of volume conduction from a single strong source or an active reference, since these influences are effectively instantaneous. The distribution is expected to be symmetric when: (i) it is flat (no coupling); (ii) when the phase difference is equal to or centers around a value of 0 mod π (influence of strong

common source/active reference). It is the second situation where the usual measures of phase synchronization will give a high value, whereas the phase lag index will give a low value. An index of the asymmetry of the phase difference distribution can be obtained from a time series of phase differences $\Phi(t)$, $t=1 \ldots N$ in the following way:

$$\mathrm{PLI} = \left|\langle \mathrm{sign}(\varphi_t)\rangle\right| \tag{5}$$

Here sign is the signum function, and we assume $-\pi <= \Phi <= +\pi$. The PLI ranges between 0 and 1: $0 <= \mathrm{PLI} <= 1$. A PLI of zero indicates either no coupling or coupling with a phase difference centered around 0 mod π. A PLI of 1 indicates perfect phase locking at a value of Φ different from 0 mod π. The stronger this non zero phase locking is, the closer to 1 PLI will be. (It does not reflect the magnitude of the phase difference.)

The directed phase lag index (dPLI)

Defined in this way the PLI is a measure of the strength of non zero phase synchronization, but no longer indicates which of the two signals is leading in phase. However, the PLI can be modified to reflect which of the two signals is leading and which is lagging in phase (mod π). Again, if we assume a time series of phase differences $\Phi(t) = \Phi_x - \Phi_y$, $t=1 \ldots N$, the directed phase lag index (dPLI) of time series x with respect to time series y can be defined as the probability $\Phi(t) > 0$. Formally:

$$dPLI_{xy} = \frac{1}{N}\sum_{t=1}^{N} H(\phi_t) \tag{6}$$

Where H is the Heaviside step function. The dPLI, like the PLI, is bounded by 0 and 1. When time series x is consistently phase leading compared to y, $0.5 < \mathrm{dPLI}_{xy} <= 1$. When time series x is phase lagging compared to y, $0 <= \mathrm{dPLI}_{xy} < 0.5$. In the case neither x or y is leading or lagging on average, $\mathrm{dPLI}_{xy} = 0.5$. Note that a relation exists between the PLI and dPLI: if $\mathrm{dPLI} = 0.5$, $\mathrm{PLI} = 0$. If $\mathrm{dPLI} = 0$, $\mathrm{PLI} = 1$, and if $\mathrm{dPLI} = 1$, $\mathrm{PLI} = 1$. The relation between PLI and dPLI can be expressed as follows:

$$\mathrm{PLI} = 2|0.5 - \mathrm{dPLI}| \tag{7}$$

The vertical bars denote the absolute value. Note that the relation between PLI and dPLI is not invertible. We can derive the PLI from the dPLI, but not the other way round.

To illustrate the use of the dPLI we consider two simple test signals that resemble a waxing and waning EEG signal (Fig. 1.). In panel A the black reference signal is consistently leading in phase compared to the blue signal. The distribution of phase differences projected on the unit circle is shown to the right. All the phase differences are in the interval $0 <= \Phi(t) < \pi$; this corresponds with a $\mathrm{dPLI} = 1$. In panel B the two signals are on average π radians out of phase. The corresponding distribution of phase differences reflects this and the dPLI is 0.46, close to the expected value of 0.5. Finally, in panel C the blue time series is phase leading compared to the black time series. Most phase differences are now in the interval $-\pi < \Phi(t) < 0$. Therefore the dPLI, computed with respect to the black signal, is 0.024, close to 0.

Description of the neural mass model (NMM)

We used a model of interconnected neural masses, where each neural mass represents a large population of connected excitatory and inhibitory neurons generating an EEG or MEG like signal. The model was described in Ponten et al. (2010) and Stam et al. (2010). The basic unit of the model is a neural mass model (NMM) of the alpha rhythm (Lopes da Silva et al., 1974; Zetterberg et al., 1978). The same neural mass model was used in a previous study on bifurcation phenomena of the alpha rhythm (Stam et al., 1999). As previously

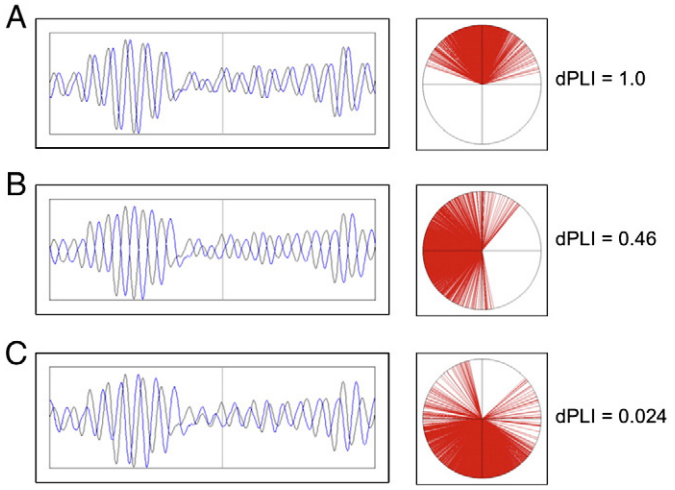

Fig. 1. Illustration of principle of directed phase lag index (dPLI). A. Left panel shows small segment of two time series where the black time series is phase-leading with respect to the blue time series. Right panel shows distribution of all instantaneous phase differences on the unit circle. All phase differences are in the upper part of the circle, between 0 and π radians. This corresponds to a dPLI of 1.0. B. Middle panel shows two time series with a phase difference that fluctuates around π radians. Right panel shows distribution of instantaneous phase differences. This distribution corresponds with $\mathrm{dPLI} = 0.46$. C. Lower panel shows the blue time series phase leading with respect to the black time series. Distribution of phase differences is shown to the right. The $\mathrm{dPLI} = 0.024$.

described, this model considers the average activity in relatively large groups of interacting excitatory and inhibitory neurons. Spatial effects are ignored in this model at the level of a single neural mass; we will introduce spatial effects later by coupling several NMMs together. The excitatory and inhibitory populations of each NMM are characterized by their average membrane potentials $\mathrm{Ve}(t)$ and $\mathrm{Vi}(t)$, and by their pulse densities, i.e. the proportion of cells firing per unit time $\mathrm{E}(t)$ and $\mathrm{I}(t)$. Static non-linear functions $\mathrm{SE}(x)$ and $\mathrm{SI}(x)$ relate the potentials $\mathrm{Ve}(t)$ and $\mathrm{Vi}(t)$ to the corresponding pulse densities $\mathrm{E}(t)$ and $\mathrm{I}(t)$. The excitatory postsynaptic potential (EPSP) and inhibitory postsynaptic potential (IPSP) are modeled by the impulse responses he(t) and hi(t). The constants C1 and C2 describe the coupling from excitatory to inhibitory and from inhibitory to excitatory populations respectively. P(t) is the pulse density of an input signal to the excitatory population. Following Zetterberg et al. (1978) the following impulse responses were used:

$$\begin{array}{ll} h(t) = A[\exp(-at) - \exp(-bt)] & \text{for } t >= 0 \\ h(t) = 0 & \text{for } t < 0 \end{array} \tag{8}$$

For $he(t)$ the parameter values were: $A = 1.6$ mV, $a = 55\ \mathrm{s}^{-1}$, $b = 605\ \mathrm{s}^{-1}$. For $hi(t)$ the parameter values were: $A = 32$ mV, $a = 27.5\ \mathrm{s}^{-1}$, $b = 55\ \mathrm{s}^{-1}$. The sigmoid function relating the average membrane potential, Vm, to the impulse density was also taken from Zetterberg et al. (1978):

$$\begin{array}{ll} S[\mathrm{Vm}-\mathrm{Vd}] = g.\exp\{q(\mathrm{Vm}-\mathrm{Vd})\} & \text{for } \mathrm{Vm} <= \mathrm{Vd} \\ S[\mathrm{Vm}-\mathrm{Vd}] = g[2-\exp\{q(\mathrm{Vd}-\mathrm{Vm})\}] & \text{for } \mathrm{Vm} > \mathrm{Vd} \end{array} \tag{9}$$

Here the parameter values used were: $q = 0.34\ \mathrm{mV}^{-1}$, $\mathrm{Vd} = 7$ mV, $g = 25\ \mathrm{s}^{-1}$. For the coupling constants we used $\mathrm{C1} = 32$ and $\mathrm{C2} = 3$ (Lopes da Silva et al., 1974). A schematic representation is shown in Fig. 2A. All model parameters are summarized in Table 1.

The final model consisted of 78 of the NMMs as described above, which were coupled together as described in de Haan et al., in press. The coupling matrix was based upon the data of Gong et al. (2009). This study described the structural connectivity between 78 AAL (automated anatomical labeling; Tzourio-Mazoyer et al., 2002) regions based upon MRI DTI in a group of 80 healthy subjects. The anatomical regions

corresponding to each of the 78 AAL regions are indicated in Table 2. In the present study, one NMM corresponded with one AAL region of the Gong et al. study. Coupling between two NMMs, if present, was always reciprocal, and excitatory. The output $E(t)$ of the main excitatory neurons of one NMM was used as the input for the impulse response he(t) of the excitatory neurons of the second NMM; the output $E(t)$ of the second module was coupled to the impulse response he(t) of the excitatory neurons of the first NMM. Following Ursino et al. (2007) we used a time delay ($T\times$ sample time, with n an integer, $0<T<21$) and a gain factor S. In the present study, n and gain were set to 1 for all connections, unless explicitly stated otherwise. A schematic illustration of the coupling between two NMMs is shown in Fig. 2.

Implementation of the model and computation of PLI and dPLI were done with the Java-based software BrainWave version 0.9.57 (available from: http://home.kpn.nl/stam7883/brainwave.html). The Java code was based on the Pascal source code described by Schuuring (Stam et al., 1999). The impulse responses, $h(t)$, were implemented as a convolution in the discrete time domain in a similar way as in the Pascal program.

The average membrane potential of the excitatory neurons Ve(t) of each of the NMMs separately was the multichannel output representing EEG signals. Thus we modeled the EEG in source space, not in sensor space. The sample frequency was 500 Hz. In the present study each run consisted of 9096 (18.19 s). Table 1 gives an overview of model parameters and initial settings. These parameters go back to large number of studies with this lumped model, and ultimately to the original model of Lopes da Silva et al. (1974). An overview of the model is shown in Fig. 2.

Table 1
Overview of model parameters.

Symbol	Interpretation	Value
t	Sample time	0.002 s
$P(t)$	Subcortical input level to each neural mass	500 spikes/s
noise	Random fluctuations around average level of P(t)	1.0
A he(t)	Amplitude of the EPSP	1.6 mV
A hi(t)	Amplitude of the IPSP	32 mV
a he(t)	Shape parameter of EPSP	55 s^{-1}
b he(t)	Shape parameter of EPSP	605 s^{-1}
a hi(t)	Shape parameter of IPSP	27.5 s^{-1}
b hi(t)	Shape parameter of IPSP	55 s^{-1}
g	Parameter of sigmoid function that relates membrane potential to impulse density	25 s^{-1}
q	Parameter of sigmoid function that relates membrane potential to impulse density	0.34 mV^{-1}
Vd1	Threshold potential used in the sigmoid function that relates membrane potential to impulse density for main population of excitatory neurons	7 mV
Vd2	Threshold potential used in the sigmoid function that relates membrane potential to impulse density for inhibitory neurons	7 mV
C1	Connection strength between main population of excitatory neurons and inhibitory neurons	32
C2	Connection strength between inhibitory neurons and main population of excitatory neurons	3
Gain	Gain factor for the coupling between different neural masses	1
T	Time delay for the coupling between neural masses	0.002 s

Description of experiments

The influence of coupling between NMM on phase patterns

This experiment investigated the spatial and temporal patterns of phase relations between the time series of the 78 neural masses as a function of coupling strength (gain parameter g in Section 2.3). Four levels of the gain factor were studied: $g=0$; $g=0.5$; $g=1$; $g=1.5$. For each level 100 epochs of 9069 samples were generated with the model using the standard settings as described in Section 2.3 and Table 1. Of each epoch of 78 time series the last 4096 samples were analyzed by computing the PLI and dPLI of the unfiltered data. The PLI and dPLI were studied at different levels of spatial and temporal resolution: (i) for each of the channels the PLI and dPLI to all other channels, averaged over 100 epochs; (ii) correlations between PLI and dPLI for $g=1$ and $g=1.5$; (iii) the detailed temporal evolution

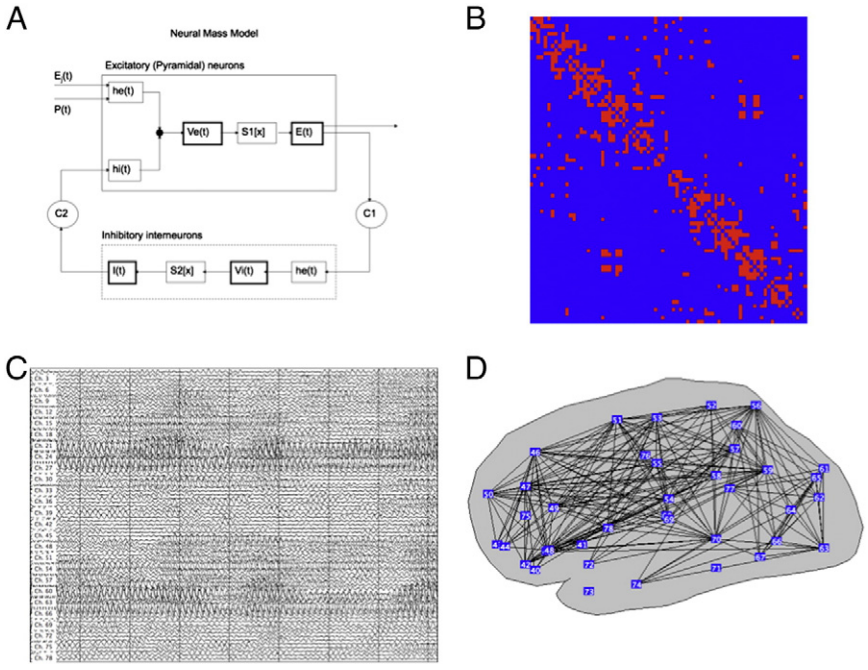

Fig. 2. Overview of the model. A. Schema of one neural mass model that simulates the average activity of interacting populations of excitatory and inhibitory neurons. The model parameters are explained in Table 1. B. All neural masses are connected according to the topology of macroscopic human network based upon DTI studies at the level of 78 AAL regions (Gong et al., 2009). C. Example of model output: each of the 78 channels corresponds to a NMM located at one of the 78 AAL positions. These time series correspond to source levels, not electrode or sensor level. D. Connectivity analysis of model output. Locations of AAL regions are projected on a sagittal view of the brain. Regions with a functional connectivity exceeding a threshold are connected by lines.

Table 2
Overview of AAL regions.

Left hemisphere		Right hemisphere	
AAL	Anatomical region	AAL	Anatomical region
1	Gyrus Rectus	40	Gyrus Rectus
2	Olfactory Cortex	41	Olfactory Cortex
3	Superior frontal gyrus, orbital part	42	Superior frontal gyrus, orbital part
4	Superior frontal gyrus, medial orbital	43	Superior frontal gyrus, medial orbital
5	Middle frontal gyrus orbital part	44	Middle frontal gyrus orbital part
6	Inferior frontal gyrus, orbital part	45	Inferior frontal gyrus, orbital part
7	Superior frontal gyrus, dorsolateral	46	Superior frontal gyrus, dorsolateral
8	Middle frontal gyrus	47	Middle frontal gyrus
9	Inferior frontal gyrus, opercular part	48	Inferior frontal gyrus, opercular part
10	Inferior frontal gyrus, triangular part	49	Inferior frontal gyrus, triangular part
11	Superior frontal gyrus, medial	50	Superior frontal gyrus, medial
12	Supplementary motor area	51	Supplementary motor area
13	Paracentral lobule	52	Paracentral lobule
14	Precentral gyrus	53	Precentral gyrus
15	Rolandic operculum	54	Rolandic operculum
16	Postcentral gyrus	55	Postcentral gyrus
17	Superior parietal gyrus	56	Superior parietal gyrus
18	Inferior parietal, but supramarginal and angular gyri	57	Inferior parietal, but supramarginal and angular gyri
19	Supramarginal gyrus	58	Supramarginal gyrus
20	Angular gyrus	59	Angular gyrus
21	Precuneus	60	Precuneus
22	Superior occipital gyrus	61	Superior occipital gyrus
23	Middle occipital gyrus	62	Middle occipital gyrus
24	Inferior occipital gyrus	63	Inferior occipital gyrus
25	Calcarine fissure and surrounding cortex	64	Calcarine fissure and surrounding cortex
26	Cuneus	65	Cuneus
27	Lingual gyrus	66	Lingual gyrus
28	Fusiform gyrus	67	Fusiform gyrus
29	Heschl gyrus	68	Heschl gyrus
30	Superior temporal gyrus	69	Superior temporal gyrus
31	Middle temporal gyrus	70	Middle temporal gyrus
32	Inferior temporal gyrus	71	Inferior temporal gyrus
33	Temporal pole: superior temporal gyrus	72	Temporal pole: superior temporal gyrus
34	Temporal pole: middle temporal gyrus	73	Temporal pole: middle temporal gyrus
35	Parahippocampal gyrus	74	Parahippocampal gyrus
36	Anterior cingulated and paracingulate gyri	75	Anterior cingulated and paracingulate gyri
37	Median cingulated and paracingulate gyri	76	Median cingulated and paracingulate gyri
38	Posterior cingulate gyrus	77	Posterior cingulated gyrus
39	Insula	78	Insula

of channel-averaged dPLI at four levels of g; (iv) the overall network configuration (averaged over all 100 epochs) at four levels of g; (v) the lagging and leading relations of two selected regions; (vi) the time series and phase distributions of two selected pairs of channels.

In the experiments described above, the delay time and coupling strength S were always the same for all possible pairs of AAL regions. Also, the couplings were bidirectional and symmetric, and the adjacency matrix was kept constant. To study the influence of varying these parameters, four further experiments were performed. In all cases the experiments were similar to the experiment described above under (i) using the average of 100 epochs and a fixed connections strength of $S=1.5$ and conduction delay of 2 ms except for the following: (1) Here the conduction delay varied between 2 and 20 ms. Conduction delay increased linearly with Euclidian distance between AAL regions. (2) Connection strength between AAL regions varied with Euclidian distance such that $S=\exp(-d_{ij})$, with d_{ij} the Euclidian distance normalized to the largest distance between any pair. (3) Connections going from left hemisphere regions to right hemisphere regions were deleted, while preserving all other connections, including left to right connections. (4) For each of the 100 epochs the original adjacency matrix was randomized using the procedure of Sporns and Zwi (2004). This preserved the degree distribution, while randomizing all other topological properties of the network. Please note that after randomization each AAL region had the same degree as before, but was now connected to randomly chosen other regions.

The influence of stimulation on phase patterns

To study the influence of stimulation of the model on the spatial and temporal distribution of phase patterns photic stimulation (presenting flashes of light to both eyes simultaneously, a standard clinical procedure to provoke epileptic activity in the EEG) was simulated. This type of stimulation has previously been shown to produce interesting dynamics in a neural mass model (Spiegler et al., 2011). To simulate photic stimulation, the thalamus to cortex input parameter Pt (spike density) was increased from the baseline level of 500 spikes/s to 800 spikes/s for the duration of one sample time (2 ms). Stimulation was only applied to the left precuneus (AAL region 25) and the right precuneus (AAL region 64). First, the stimulation frequency that induced the largest change in PLI and dPLI was determined by stimulation the model with a range of frequencies from 1 to 18 Hz in 1 Hz steps. For each stimulus frequency the PLI and dPLI per channel was averaged over 10 runs. Next, the spatial and temporal patterns of dPLI averaged over 100 epochs and using a coupling gain $g=1$ were studied with the optimal stimulus frequency. In addition, the average evoked potential, obtained by averaging the time series of each of the 100 epochs, was subjected to spatial and temporal dPLI analysis.

Results

The influence of coupling between NMM on phase patterns

The influence of different levels of coupling between the 78 NMM on spatial temporal phase patterns was investigated by computing the PLI and dPLI of the model time series. The PLI and dPLI, averaged for each AAL region to all other regions and averaged over 100 epochs, is shown in Figs. 3A and B. In the case of absent coupling (gain parameter $g=0$) or weak coupling ($g=0.5$) the PLI fluctuates around 0.1, with little or no consistent regional differences. In contrast, a clear pattern emerges for higher coupling levels ($g=1$ and $g=1.5$). The average PLI increases from 0.087 (for $g=0$) and 0.098 (for $g=0.5$) to 0.25 (for $g=1$) and 0.247 (for $g=1.5$). In addition a spatial pattern emerges, especially for an intermediate coupling strength ($g=1$). At this coupling strength the lowest PLI values are found at the left olfactory cortex (AAL 2) and Heschl gyrus (AAL 29), and in the right hemisphere the gyrus rectus (AAL 40), orbital part of the middle (AAL 44) and inferior (AAL 45) frontal gyrus, Heschl gyrus (AAL 68), temporal pole of the superior temporal gyrus (AAL 72) and insula (AAL 78). The highest PLI values are found at the left superior parietal gyrus (AAL 17), precuneus (AAL 21), calcarine fissure and surrounding cortex (AAL 25), cuneus (AAL 26), and the right precuneus (AAL 60), superior occipital gyrus (AAL 61), calcarine fissure and surrounding cortex (AAL 64) and cuneus (AAL 65). For a coupling strength of $g=1.5$ a similar but less outspoken pattern of PLI distribution can be seen.

For absent coupling ($g=0$) and weak coupling ($g=0.5$) the dPLI is 0.5 for all regions (Fig. 3B). Again a spatial pattern emerges at higher coupling strengths. For $g=1$ minima of dPLI are found in the left hemisphere at the precuneus (AAL 21), superior occipital gyrus (AAL 22), calcarine fissure and surrounding cortex (AAL 25) and cuneus (AAL 26), and in the right hemisphere at the precuneus (AAL 60), superior occipital gyrus (AAL 61), calcarine fissure and surrounding cortex (AAL 64) and the cuneus (AAL 65). The pattern of dPLI minima is similar but less outspoken at a coupling strength of $g=1.5$. For both coupling strengths dPLI values >0.5 are distributed more smoothly over anterior brain regions.

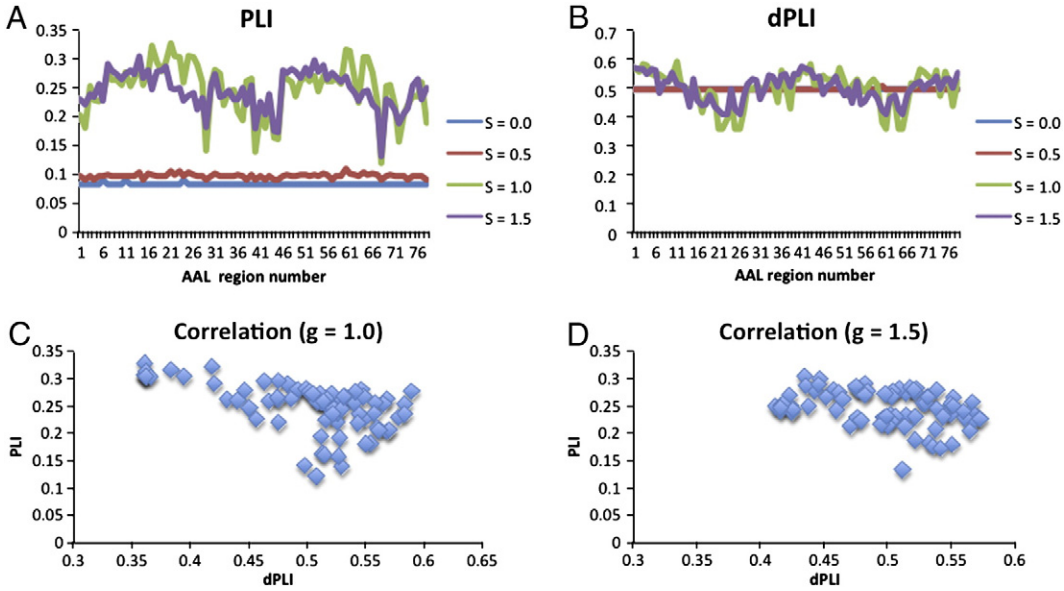

Fig. 3. A. Plot of PLI for different levels of coupling strength S for each AAL region (see table for the anatomical areas corresponding to the AAL regions). Results are average over 100 runs. B. Plot of dPLI for different levels of connection strength S for each AAL region. Results are average over 100 runs. C. Correlation between dPLI and PLI for coupling strength $g = 1.0$. D. Correlation between dPLI and PLI for coupling strength $g = 1.5$.

Correlations between dPLI and PLI (averaged per region and over 100 epochs) at coupling strength $g = 1$ and $g = 1.5$ are shown in Figs. 3C and D. For $g = 1$, dPLI values that are much lower or higher than 0.5 are associated with high PLI values; dPLI values around 0.5 do not show a particular association with either low or high PLI values. For $g = 1.5$ no clear correlation between dPLI and PLI is evident.

We also determined correlations (at a significance level $p<0.01$) between PLI as well as dPLI per region and structural network measures such as betweenness centrality, degree, clustering coefficient, path length and node vulnerability as reported by Gong et al. (2009, Supplementary Table 2). In the case of PLI for $g = 0$ no significant correlations with any of the structural measures were present. For a coupling gain $g = 0.5$ and $g = 1.0$ a significant positive correlation was present between PLI and betweenness centrality, degree and vulnerability, and a negative correlation with nodal path length. For $g = 1.5$ the PLI correlated positively with degree and vulnerability, and negatively with path length. For $g = 0$ the dPLI did not correlate with any of the structural measures. For $g = 0.5$ the dPLI showed positive correlations with betweenness, degree and vulnerability. For $g = 1.0$ and $g = 1.5$ dPLI correlated negatively with betweenness, degree and vulnerability, and positively with nodal path length.

To gain a better understanding of these results, in particular the dependence on coupling strength of the dPLI/topology correlations, we considered a simple star graph with one central neural mass connected to 20 other neural masses (Fig. 4A). In this simple model the central node had degree 20 and the highest centrality. As shown in Fig. 4B the high degree central node was weakly leading in phase for weak coupling, but became strongly phase lagging for strong coupling, with a transition between the two types of behavior at a coupling strength of 2. PLI increased with coupling strength, but showed a relative dip at a coupling strength of 2. A similar phenomenon may occur in the full model at a lower coupling strength between $g = 0.5$ and $g = 1.0$.

Next we examined spatial and temporal dPLI patterns in more detail. In Fig. 5 the dPLI for each region as a function of time is illustrated for four levels of coupling strength. In this case the dPLI of a region at a specific time is defined as the probability that the phase of the time series of that region at that time is leading (modulo π) compared to the phase of the 77 other regions. At a coupling strength of $g = 0$ (panel A) almost no structure is seen apart from some minimal fluctuations. At a coupling strength of $g = 0.5$ (panel B) structure starts to emerge in the dPLI plot. In the first second, between 3.5 and 4.5 s, and after 7.5 s red (phase leading) and blue (phase lagging)

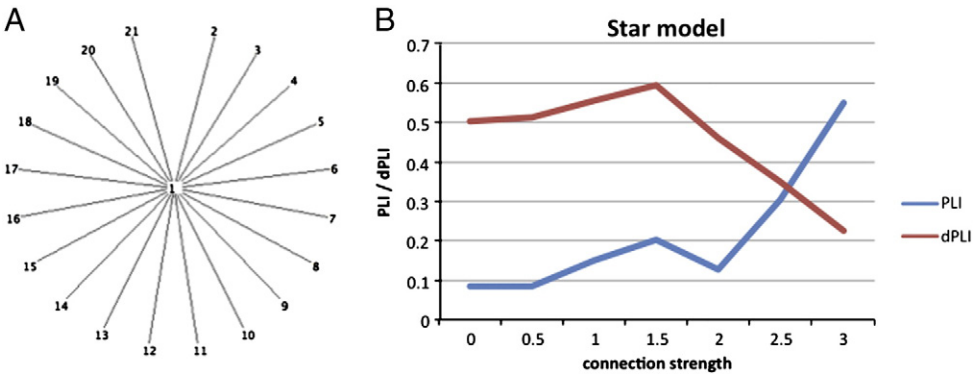

Fig. 4. Dependence of PLI and dPLI on connection strength in a simple star graph. A. Schema of the star graph with one central NMM and 20 surrounding neural masses. B. PLI and dPLI (averaged over ten runs) of central neural mass as function of coupling strength.

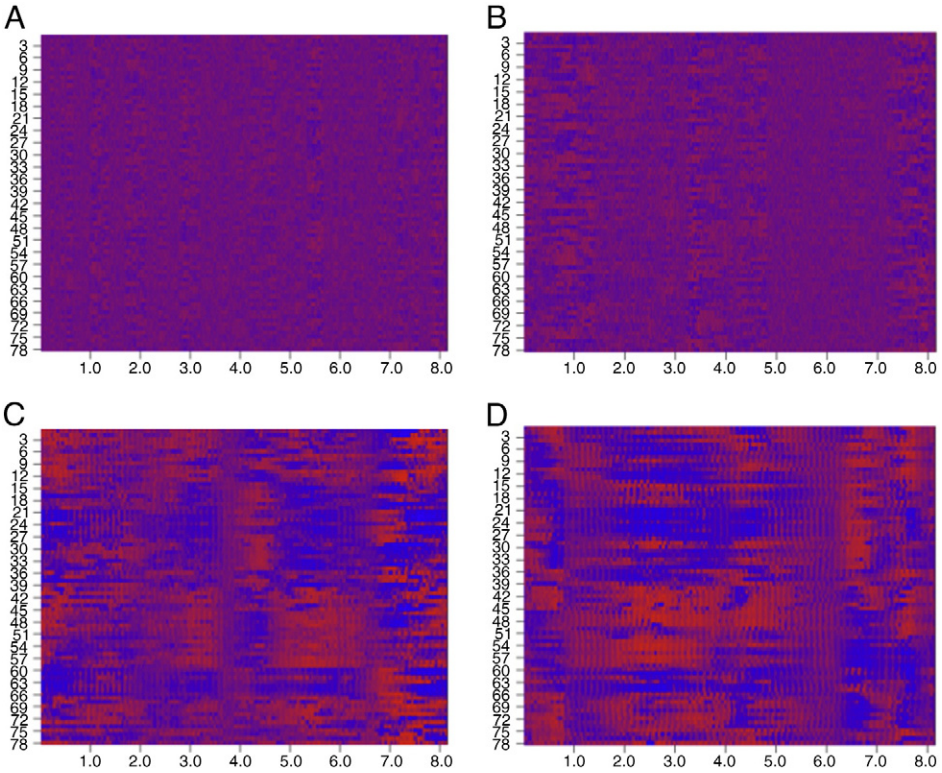

Fig. 5. Temporal evolution of dPLI for all 78 AAL regions for a single epoch. Numbers on the *Y*-axis correspond to AAL regions. *X*-axis corresponds to time in seconds (sample frequency 500 Hz; input level = 500 spikes/s). Red color means phase leading, blue color means phase lagging. A. Connection strength $S = 0$; B. Connection strength $S = 0.5$; C. Connection strength $S = 1.0$; D. Connection strength $S = 1.5$.

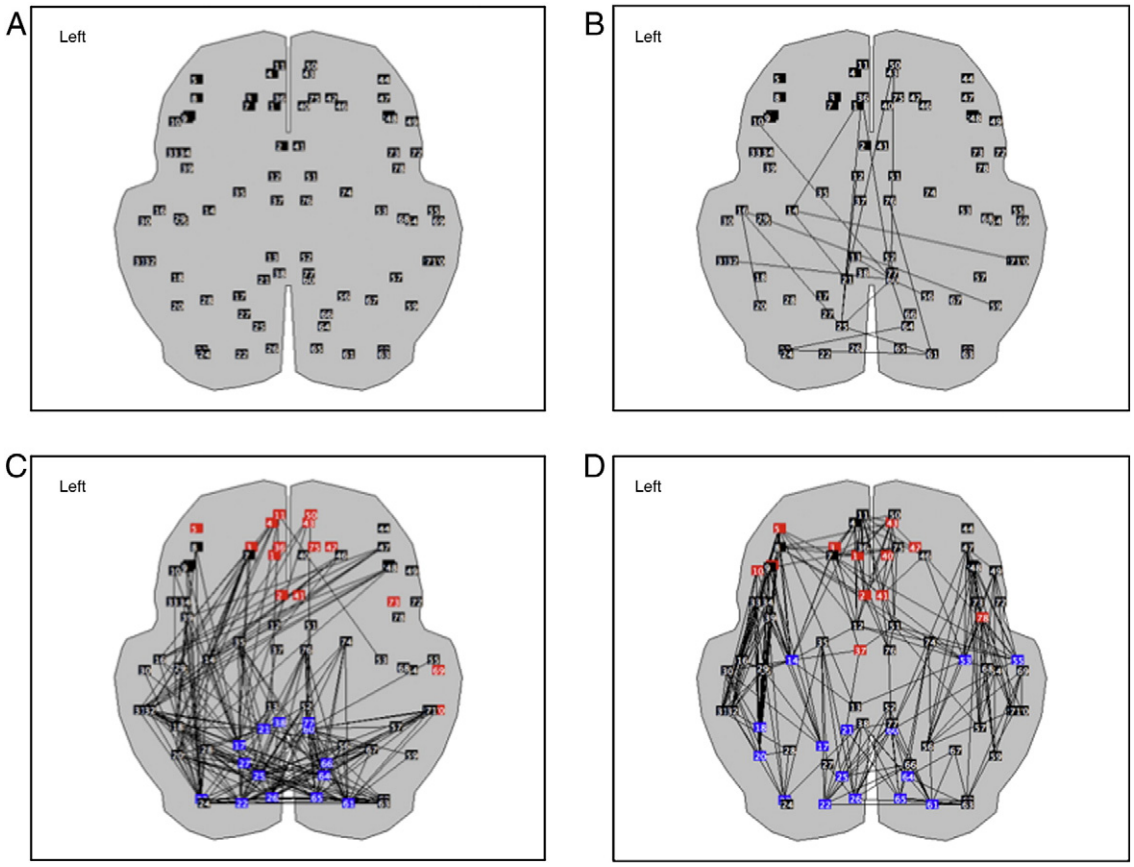

Fig. 6. Distribution of dPLI of AAL regions for four levels of the connection strength S (A: $S = 0$; B: $S = 0.5$; C: $S = 1.0$; D: $S = 1.5$). Blue indicates dPLI < 0.45; black 0.45 < dPLI < 0.55, and red dPLI > 0.55. Lines between regions correspond to PLI values > threshold. Results are average of 100 runs. Transversal view. Anatomical regions corresponding to the AAL numbers are described in Table 2.

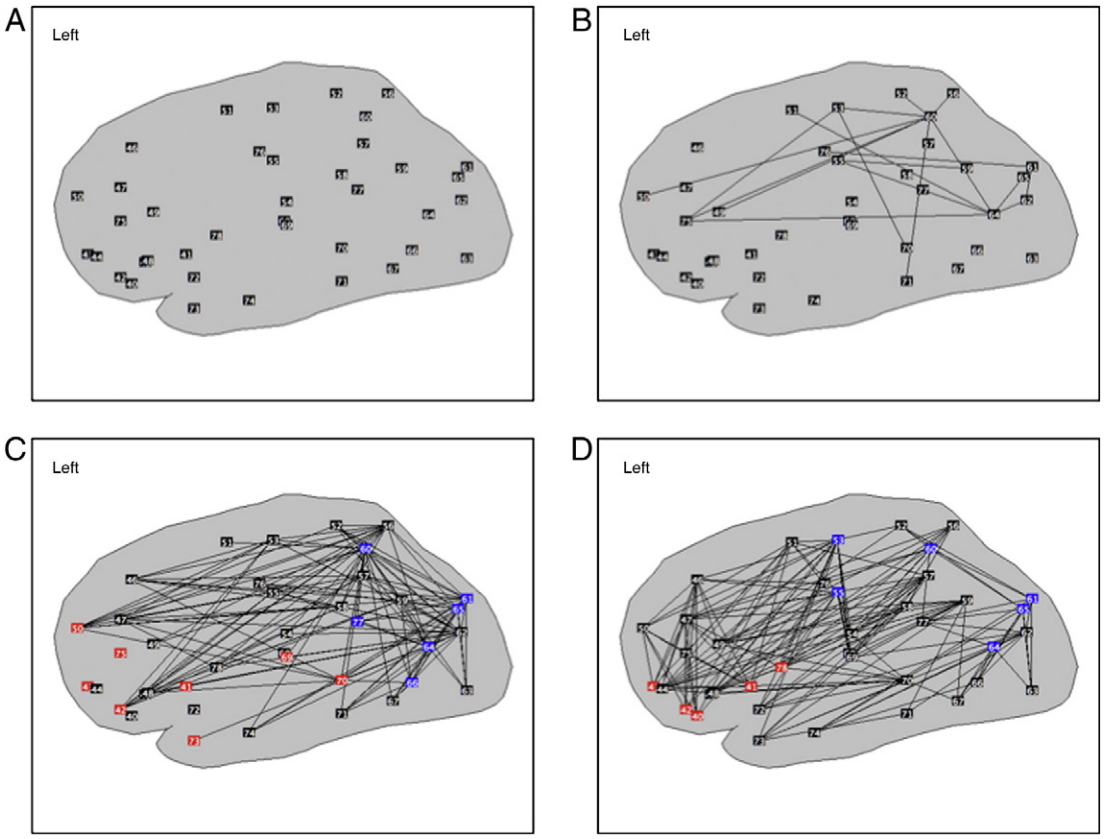

Fig. 7. Same as Fig. 3. Sagittal view.

clusters of regions appear. These episodes are separated by blurred intervals with little or no distinguishable patterns of phase leading and lagging. For a coupling strength $g = 1$ (panel C) a clear alternation between episodes with large clusters separated by shorter blurred episodes can be seen. At the highest coupling level of $g = 1.5$ (panel D) a similar pattern can be observed. Note that regions belonging to a phase leading cluster at one time may participate in a phase lagging cluster at a later time. The characteristic time scale of the phase leading and lagging clusters is of the order of a few hundred milliseconds.

The spatial pattern of dPLI based upon averaging over 100 epochs is shown in Figs. 6–8. For the purpose of illustration, areas with an average dPLI < 0.45 are shown in blue, those with an average dPLI > 0.55 are shown in red. For 0.45 < dPLI < 0.55 areas are shown in black. At coupling strengths of $g = 0$ and $g = 0.5$ no regions with clear phase leading or lagging are evident. At a coupling strength of $g = 1$ a clear pattern can be seen. Frontal regions in the left (AAL regions 1, 2, 3, 4, 5, 11, 36) and right (AAL regions 41, 40, 43, 50, 69, 70, 73, 75) hemisphere are phase leading. Posterior medical and occipital regions in the left (AAL regions 17, 21, 22, 23, 25, 26, 27, 38) and right (AAL regions 60, 61, 64, 65, 66, 77) hemisphere are phase lagging. At a higher coupling strength of $g = 1.5$ a similar pattern can be seen, but now phase leading areas in particular can be seen in more anterior brain regions in the left (AAL regions 14, 18, 20) and right (AAL regions 53, 55) hemisphere.

So far we have considered the average dPLI for each region, that is the average of the pair wise dPLIs of a region and all other regions. Next we consider two regions, one leading (AAL region 11, left medial superior frontal gyrus) and one lagging (AAL region 21, left precuneus), in more detail (Fig. 9) at a coupling level $g = 1.0$. As shown in Fig. 9, panel A, the left medial superior frontal gyrus is phase leading with respect to many areas in the whole left hemisphere, and with respect to a few scattered areas in the right hemisphere. In contrast, as shown in panel B, this brain area is lagging in phase compared to a smaller number of areas in the right hemisphere. The left precuneus is only phase leading with respect to the left middle frontal gyrus, pars orbitalis (AAL region 5) and superior occipital gyrus (AAL region 22) (panel C). The left precuneus is lagging in phase compared to a large number of other areas widely distributed in *both* hemispheres (panel D). The pattern of phase lagging of the left precuneus compared to the left gyrus lingualis is shown in Fig. 10, panel A. In Fig. 10, panel B, the phase leading of the left medial superior frontal gyrus with respect to the left precentral gyrus is illustrated. For both examples the actual distribution of the phase differences is shown on the right. Note that the extent of phase leading and lagging may change over time, in agreement with the observations on temporal evolution of dPLI in Fig. 5.

The results of four experiments investigating the effect of varying various connectivity parameters are shown in Fig. 11. In Fig. 11A the results of varying the conduction delay between 2 and 20 ms depending on the Euclidian distance between AAL regions are shown. While the range of dPLI values is slightly lower than in Fig. 6, a similar pattern can be seen with frontal regions phase leading and median and posterior regions phase lagging. Fig. 11B shows the results for using connection strengths that decrease exponentially with distance. Here a clear front-to-back pattern can be seen that involves many midline regions as well as a few more lateral areas. As shown in Fig. 11C deleting the connections from left to right hemisphere regions (but not the other way around) produces a pattern of right frontal to left posterior phase differences. Finally, Fig. 11D shows that randomizing the adjacency matrix while preserving the degree distribution (and the degrees of all individual AAL regions) does not disrupt to anterior to posterior phase shift.

The influence of stimulation on phase patterns

To investigate the influence of stimulation on the distribution of phase differences we simulated photic stimulation of the visual

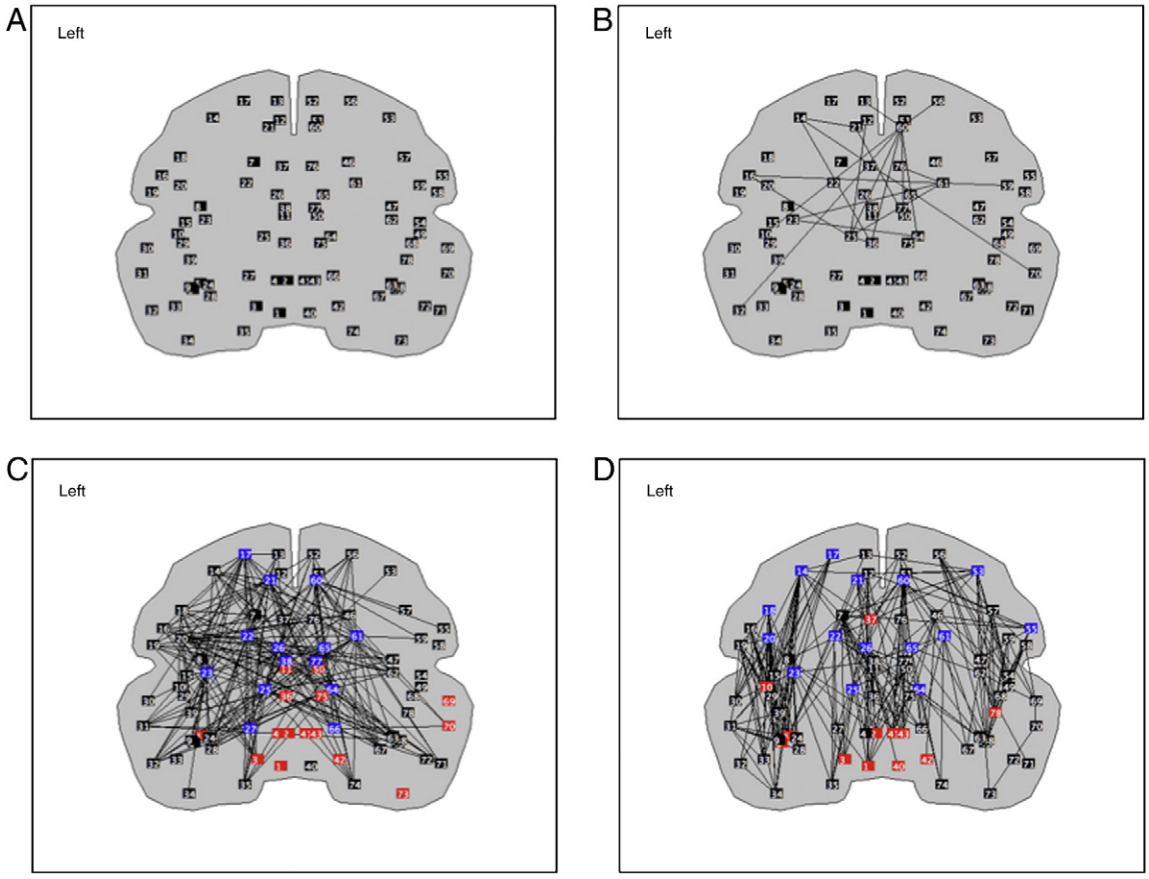

Fig. 8. Same as Fig. 3. Coronal view.

areas around the left and right calcarine sulcus (AAL region 25 and 64). First we determined the stimulation frequency that caused the largest change in average PLI and range of dPLI (over all regions). As shown in Fig. 12, the largest increase in PLI and the largest range of dPLI was found for a stimulation frequency of 9 Hz. Average PLI and dPLI at the stimulation frequency of 9 Hz and a coupling gain $g = 1.0$ for all 78 regions are shown in Fig. 12 panel B. From this figure it is clear that PLI and dPLI vary strongly between regions. The spatial pattern of dPLI is shown in Fig. 13. It is evident that many regions scattered throughout the brain, including the stimulated areas around the left and right calcarine sulcus (AAL 25 and 64) are now phase leading. In the transversal view many phase lagging areas throughout the brain seem are evident as well. Of interest, the sagittal and coronal views reveal a remarkable pattern where the driving regions are almost all located in the lower orbito frontal, temporal and occipital part of the brain whereas the lagging regions are located mostly in the upper superior frontal, central and parietal part of the brain. The three panels at the bottom of Fig. 12. show that a very similar pattern is observed when the dPLI is computed from the average evoked visual response instead of the dPLI averaged over time series of the 100 epochs. The 78 channel average evoked response is shown in Fig. 14, panel A, with the channels corresponding to the stimulated brain areas shown in red. The average evoked response has the shape of a sine with a frequency of 9 Hz. Remarkably, there is a delay in the emergence of the response in areas further away from the stimulated region. Also, the average evoked response has a lower amplitude in distant channels. Fig. 14B shows the time evolution of the dPLI for all channels. After onset of stimulation there is first a transient of about 1 s. Subsequently there is a clear pattern of phase leading channels (in red) and phase lagging channels (in blue), corresponding to the pattern shown in Fig. 13.

Discussion

This study showed that in the case of sufficient average connection strength a characteristic “front-to-back” pattern of phase differences, with medial frontal regions leading and medial parietal and occipital regions lagging, emerges naturally in a model of neural masses connected in agreement with data from a human DTI study (Gong et al., 2009). The full model as well as a simple star model showed that brain areas with higher centrality had stronger connectivity to other regions. Regions with high centrality were leading other regions at weak coupling strength, but lagging strongly at high coupling strength. Detailed analysis of this pattern using a directed phase lag index (dPLI) revealed a sequence of states, each lasting about a few hundred milliseconds, with a stable distribution of leading and lagging clusters. Individual areas displayed differences in the pattern of their phase relations with other regions in the same or the contralateral hemisphere. Stimulation of the primary visual areas at 9 Hz reversed the “front-to-back” pattern and resulted in the occipital and basal temporal areas leading, and the dorsal frontal and central areas lagging in phase. Analysis of the average evoked response confirmed this result.

The emergence of a consistent “front-to-back” pattern of phase differences at sufficient coupling strength is a remarkable and somewhat unexpected outcome although it fits surpisingly well with previous observations on anterior to posterior phase delays of gamma activity and delta waves (Llinás and Ribary, 1993; Massimini et al., 2004). It should be stressed that all 78 neural masses were identical, and all connnections between neural masses were bidirectional, excitatory and of equal strength. However, a neural mass with more connections to other regions, receives more excitatory input, increasing its firing density and oscillatory power, and its functional connectivity to other regions. This explains the correlation between topological measures

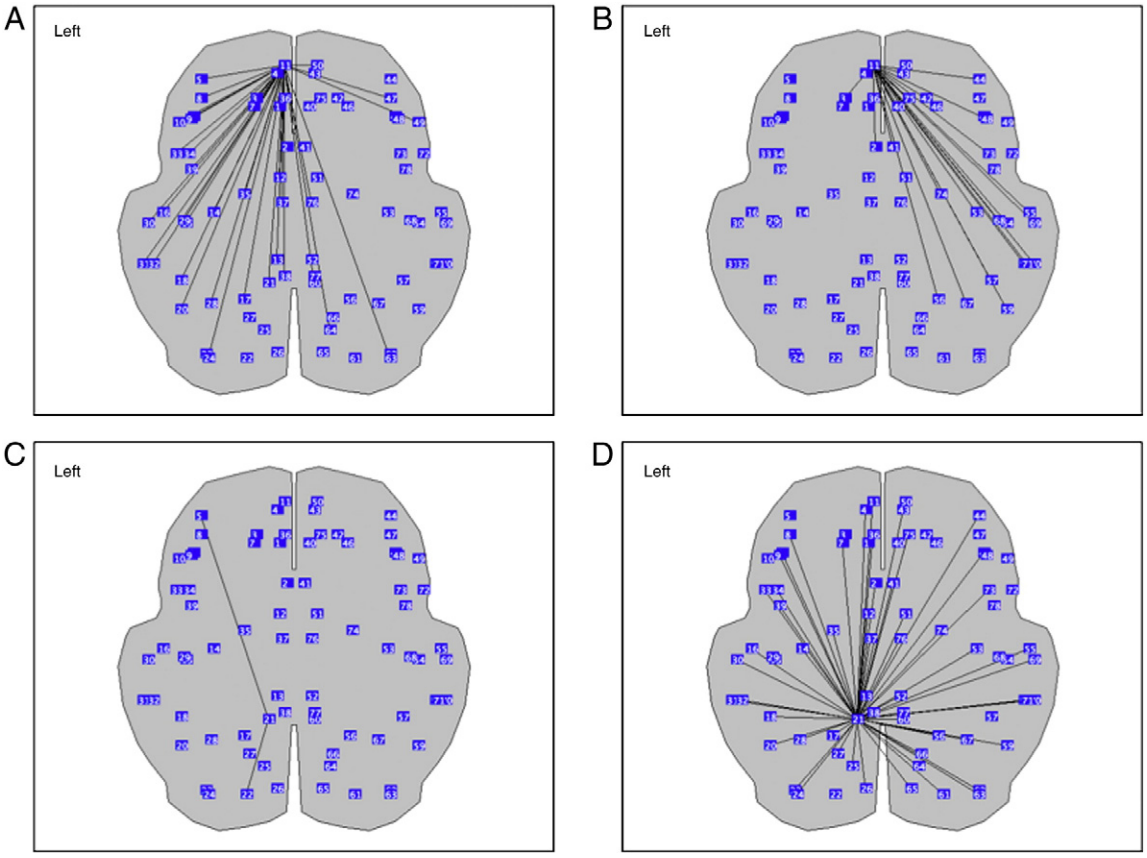

Fig. 9. Details of dPLI networks centered around AAL region 11 (SFGmed left) and AAL region 21 (PCUN left). A. Areas where SGFmed left is phase leading (dPLI > 0.55). B. Areas where SFGmed is phase lagging (dPLI < 0.45). C. Areas where PCUN left is phase leading (dPLI > 0.55). D. Areas where PCUN left is phase lagging (dPLI < 0.45). (S = 1; Input level = 500 spikes/s).

of centrality such as degree and betweenness and a high PLI. To understand the relation between topological characteristics and dPLI we considered 21 NMM coupled in a simple star network (Fig. 4). At weak coupling strength the central NMM, with the highest degree and betweenness centrality, was weakly leading, whereas the same NMM was strongly lagging at high coupling strengths. This suggests that the front-to-back pattern observed in the full model might be the result of lower centrality of areas belonging to the anterior part of the default mode network, and higher centrality of areas belonging to the posterior part of the default mode network. It also explains why this pattern only becomes evident at a high coupling gain g.

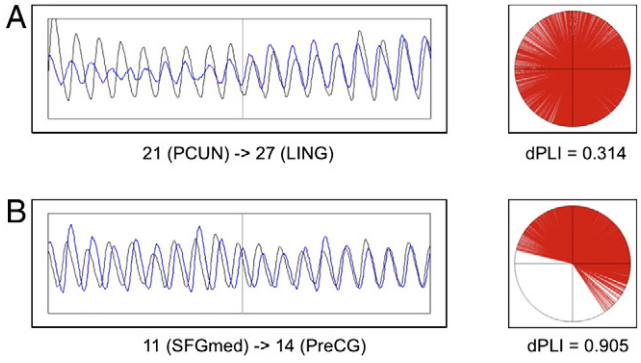

Fig. 10. Details of phase relation between two pairs of areas. Phase distributions and dPLI values are shown on the right. A. Coupling between area 21 (PCUN left) and are 27 (LING left). B. Coupling between area 11 (SGFmed left) and area 14 (PreCG left). (S = 1; Input level = 500 spikes/s).

Although the "front-to-back" pattern of the model may seem surprising, it is in agreement with empirical EEG and MEG studies. During sleep a characteristic pattern of delta waves emerging in the (left) frontal regions and spreading from there to more posterior areas has been demonstrated (Massimini et al., 2004). Triphasic waves in the EEG, associated with hepatic encephalopathy, also display a characteristic pattern with frontal regions leading in phase compared to more posterior regions (Boulanger et al., 2006). Llinás and Ribary (1993) demonstrated an anterior to posterior phase shift of MEG gamma band oscillations during wakefulness and NREM sleep. Apparently a "front-to-back" pattern of phase differences can arise under different normal as well as pathological conditions. The important conclusion from the model simulations is that such a pattern could be a natural result of the topological organization of human brain networks at the macroscopic level.

Remarkably all regions with strong functional connectivity and strong phase leading or lagging are part of the default mode network, or are closely associated with it. The default mode network is known to be most active during a resting-state. It is assumed to constitute a "connectivity backbone" or "rich club" that is closely associated with internal processing of information and intelligence (Van den Heuvel and Sporns, 2011). Abnormalities of the default mode network have been associated with several neuropsychiatric disorders, notably Alzheimer's disease and loss of consciousness (Hafkemeijer et al., 2012; Soddu et al., 2011). The dynamics of the model without stimulation can be considered an approximation of the resting-state. The model shows that high levels of activity and strong functional connectivity of areas belonging to the default mode network emerge naturally solely due to the topological organization of the brain. In addition the model suggests that in a resting-state information may flow preferentially from the anterior part of the default mode network to its posterior part as shown previously for gamma and delta band oscillations (Llinás and

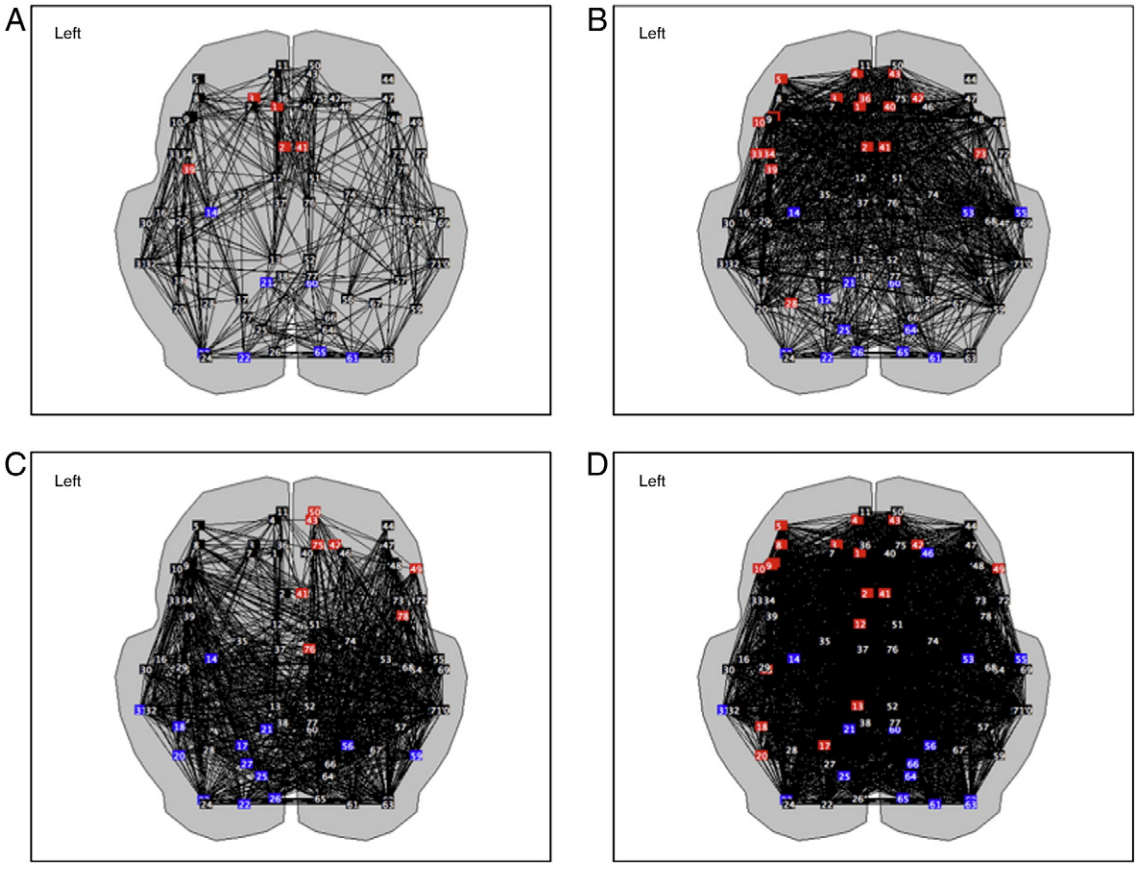

Fig. 11. Influence of variation of connectivity parameters on phase patterns. Results are average of 100 runs, with connection strength S = 1.5 unless indicated otherwise, conform the procedure used for Figs. 6–8. A. Conduction delay between all pairs of AAL regions varies between 2 and 20 ms. Conduction delay is linearly correlated with Euclidian distance between AAL regions. B. Strength of coupling between all AAL regions decays exponentially with Euclidian distance ($S = 1.5 * \exp(-d_{ij})$, where d_{ij} is the Euclidian distance between region i and j normalized to the largest distance between any pair). C. All connections between AAL regions in the left hemisphere to AAL regions in the right hemisphere set to zero. All other connections (including those from the right to the left hemisphere) have strength $S = 1.5$. D. Phase distribution patterns after randomizing the original adjacency matrix while preserving the degrees of all AAL regions.

Ribary, 1993; Massimini et al., 2004). This is in line with the default mode network plays a crucial role in the monitoring of the self and internal thoughts during the resting-state.

Previous model studies have shown that topological patterns of functional connectivity may resemble structural connectivity at long time scale, but may display a different organization at shorter timescales.

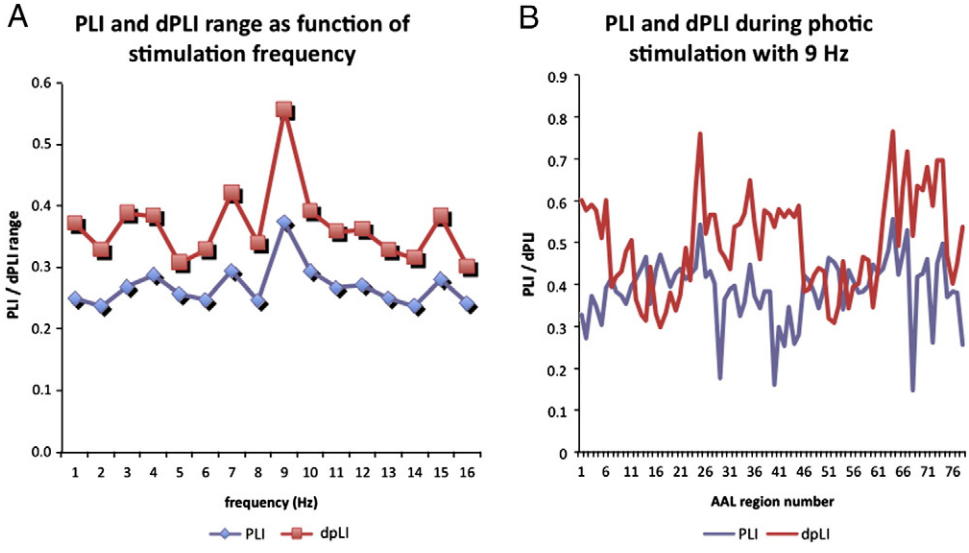

Fig. 12. Influence of photic stimulation on PLI and dPLI. Photic stimulation consisted of increasing the input level from 500 to 800 spikes/s for 2 ms. Stimulation was applied to AAL area 25 (CAL left) and 64 (CAL right). A. PLI (average of all areas) and dPLI (range of dPLI of all areas) as a function of photic stimulation frequency. Results are averaged over 10 runs. B. PLI and dPLI for all 78 AAL regions for photic stimulation with 9 Hz. Results are averaged over 100 runs.

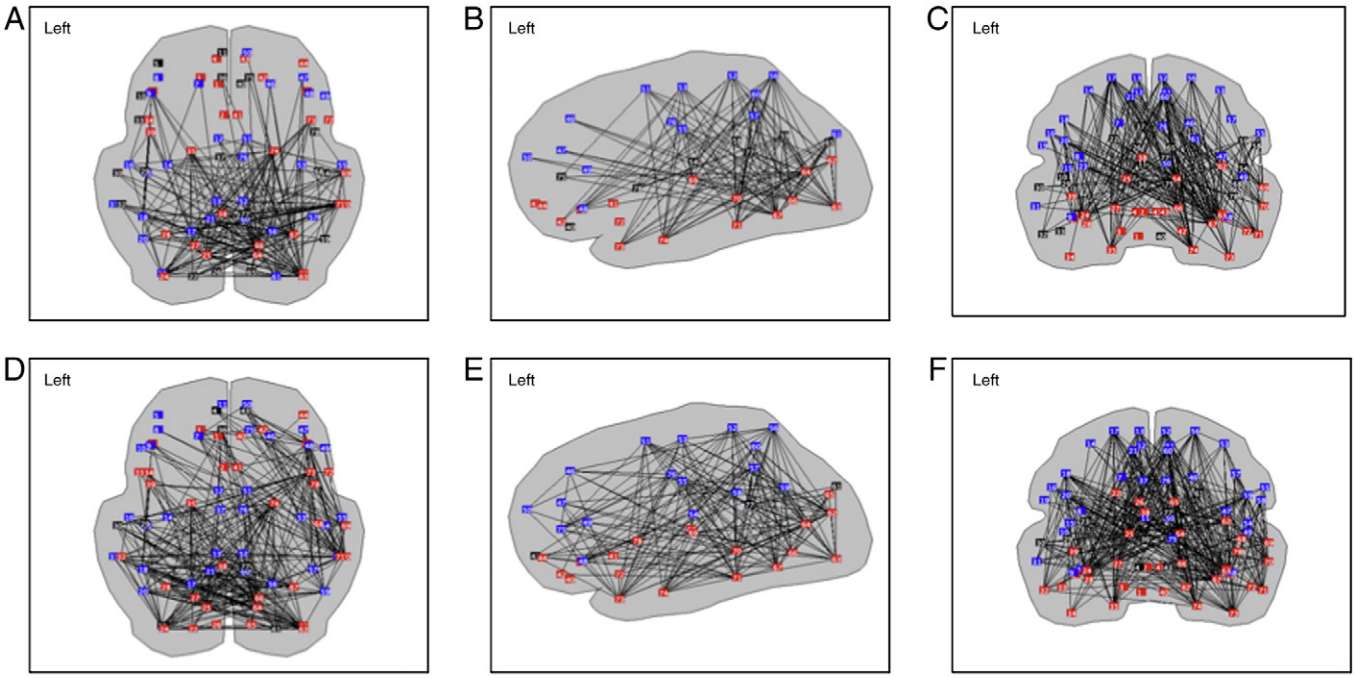

Fig. 13. Influence of photic stimulation with 9 Hz of AAL area 25 (CAL left) and 64 (CAL right) with spike of 800 for one sample (S = 1; Input level = 500 spikes/s). Upper row shows average PLI and dPLI (dPLI > 0.55 in red; dPLI < 0.45 in blue). Lower row shows results of PLI and dPLI applied to average evoked response (averaged over 100 epochs). Visual regions are now leading rather than lagging in phase.

Honey et all showed that functional connectivity resembles structural connectivity at timescale of about a minute. On time scale of many seconds anti correlated functional networks emerged, while rapidly changing functional networks were seen at sub second timescales. In our study averaging over long timescales (8192 s, 13.65 minutes) resulted in stable patterns of functional connectivity and phase relations. Analysis of directed phase lag patterns at millisecond resolution showed a remarkable pattern of short episodes, each lasting about a few hundred milliseconds, each consisting of a characteristic distribution of phase leading and phase lagging clusters of brain regions. These patterns are in agreement with the observations of Honey et al. at short time scales. Moreover, there seems to be a possible connection between our episodes of stable phase leading and lagging clusters and the notion of microstates as introduced by Lehmann et al. (2006). Recent work combining EEG with fMRI suggests that microstates may be subsecond states of semi stable electro magnetic patterns corresponding with activation of one of the resting-state networks (Musso et al., 2010). Of interest, our model study suggests that microstate-like patterns can emerge spontaneously through an interaction of network topology and neural mass dynamics. If the global connection strength is sufficiently strong the brain may have a natural tendency to subsequently activate different subnetworks.

A detailed analysis of a typical phase leading and a typical phase lagging region showed remarkable qualitative differences. The left medial superior frontal gyrus, part of the anterior default mode network, is a typical example of a phase leading region (Fig. 9). This area was leading in phase to many other regions, all of which were located in the same hemisphere. This area in its turn was also driven by a number of other areas, all of which were located in the contralateral hemisphere. The left precuneus, part of the posterior default mode network, showed a rather different pattern. It was only leading two other areas in the same hemisphere, and was driven by a large number of brain regions from both hemispheres (Fig. 9). The functional significance of these qualitative differences is not yet clear. One might speculate that the left medial frontal gyrus acts as a kind of intermediate station, a "connector hub", between large networks in the contralateral and ipsilateral hemisphere. In contrast, the left precuneus seems to function

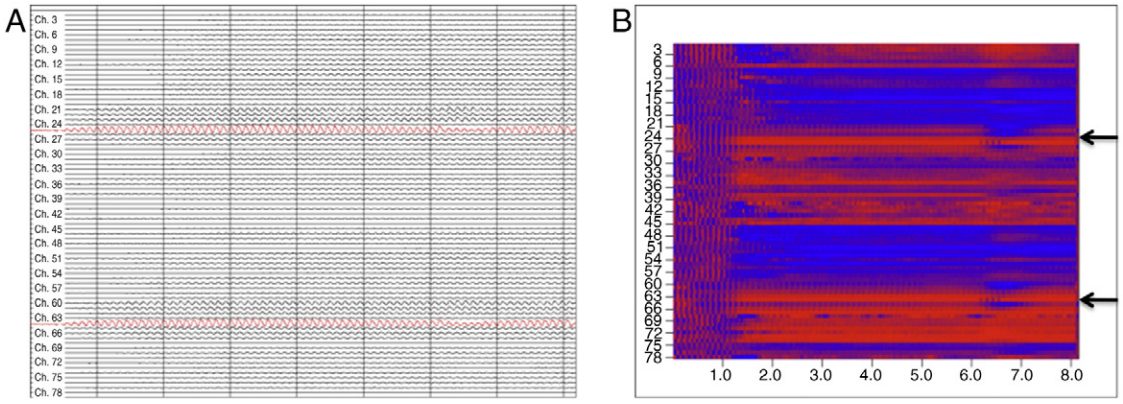

Fig. 14. A. Average evoked response based upon 100 epochs with photic stimulation with 9 Hz. Channels in red correspond to stimulated areas (AAL area 25, CAL left; AAL area 64, CAL right).B. Spatial temporal evolution of dPLI of the average evoked response of A. The two black arrows correspond to the stimulated areas. Numbers on the *Y*-axis correspond to AAL regions. *X*-axis corresponds to time in seconds.

mainly as an integrator of information of large parts of both hemispheres. We have analyzed only two regions in detail by way of example, but it is conceivable that analysis of other regions may reveal different profiles of phase relations. However, it is important to validate the predictions of the model by empirical observations on functional brain networks in source space (Hillebrand et al., 2012).

As shown in Fig. 11 the front-to-back pattern described above could not be explained by the fact that we used fixed conduction delays and connections strengths, or symmetric reciprocal connections. Varying the conduction delays or connections strengths in a distance dependent way did not disrupt the anterior to posterior phase shift. Disrupting the connections between left hemisphere regions and right hemisphere regions (but not the other way around) induces a right frontal to left posterior pattern. Finally, randomizing the adjacency matrix while preserving the degree distribution and the degrees of the individual AAL regions did not disrupt the front-to-back phase pattern. This suggests that the degrees of the AAL regions, as well as their position in the brain network, but not other higher order topological properties, can explain the distribution of phase leading and phase lagging regions.

To check the validity of the model, and the reliability of the phase difference patterns revealed by the directed phase lag index, we simulated the effect of a relatively simple type of stimulation. Photic stimulation is routinely used in clinical EEG studies to excite the visual system and provoke epileptiform EEG abnormalities in patients suffering from certain types of epilepsy. Stimulation exists of strong flashes administered to both eyes at different frequencies. We simulated this process by very briefly increasing the input of the areas surrounding the calcarine sulcus. The strongest effect on both PLI and dPLI was found for stimulation with 9 Hz, slightly below the intrinsic frequency of the visual areas. One would expect that strongly stimulated brain areas would drive other areas to which they are connected (Palva et al., 2011). Indeed this is what we observed in the model (Fig. 13). The "front-to-back" pattern of the resting-state was now reversed, and the visual areas were phase leading with respect to the other more frontal and dorsal areas. This suggests that the directed phase lag index does reflect the direction of information flow under well controlled conditions, in agreement with empirical studies (Palva et al., 2011).

Unexpectedly, visual stimulation not only reversed the "front-to-back" pattern, but also resulted in a separation between phase leading basal temporal / occipital areas, and phase lagging dorsal fronto central areas (Fig. 13). This pattern has some resemblance to the distinction ventral and dorsal stream of visual information flow. The most likely explanation is that this pattern is a fundamental property of the structural brain networks, and becomes evident at the functional level if the primary visual areas are stimulated. It suggests that the model, in combination with directed phase lag analysis, could be used to track approximately the flow of information when stimulating other brain regions of interest. Analysis of spatial dPLI patterns was based upon averaging the dPLI values of all regions for each epoch. As a further check we computed the average evoked visual response (Fig. 14). This corresponds to a steady-state visual evoked potential. Analysis of the average evoked visual response confirmed the findings derived from averaging the dPLI patterns of the individual epochs. In addition it revealed after onset of visual stimulation there is a transient of about seconds before the response becomes stable.

In the present study we used a novel measure, the directed phase lag index (dPLI) to study patterns of phase differences between signals generated by neural masses. The dPLI is derived from the phase lag index (PLI), which measures the strength of phase coupling between two time series while avoiding the bias due to volume conduction and active reference electrodes (Stam et al., 2007). The dPLI and PLI are closely related. In fact, the dPLI uses information about the distribution of the instantaneous phase differences that is also used for the computation of the PLI. In contrast to the PLI, the dPLI takes into account asymmetric phase relations, and thus identifies which channel is leading and which channel is lagging in phase. It should be stressed however that this identification can be ambiguous, since leading with a small phase difference φ is the same as lagging with a large phase difference $\pi-\varphi$. Identification of the leading channel can therefore be difficult, especially for high frequencies, but for frequencies in the alpha band, such as in the present model, interpretation is possible if biological information about conduction delays is taken into account. Conduction delays in cortical networks probably are probably smaller than 40 ms, while a typical alpha wave lasts 100 ms. This fact, in combination with the observations from photic stimulation, suggest that dPLI values >0.5 most likely identify phase leading rather than phase lagging areas.

We should stress that the existence of a consistent phase difference between the time series of two regions by itself does not allow an interpretation in terms of causal influence. Effective connectivity refers to such causal influences of one region on another, and requires special methods, often based upon directed transfer or Granger causality (Gourévitch et al., 2006). While these measures are of considerable interest, they tend to be more complicated than the dPLI. Also, they may be less suitable to study the temporal evolution of asymmetric interactions which can be easily done with the dPLI (Fig. 5b). There are strong suggestions that consistent and small phase differences, tuned to typical conduction times, are important for information exchange between populations of oscillating neurons (Fries, 2005). Within the context of studying patterns of phase relations between oscillatory signal from neural populations the dPLI may therefore present a simple and attractive measure to track the flow of information.

Conclusions

We have shown that a directed phase lag index can be used to study the spatial and temporal patterns of phase relations in a realistic model of macroscopic structural and functional brain networks. The results of model simulation confirm and explain some well known facts, such as the high level of activity of the default mode network. The model makes also a number of predictions that require empirical studies for confirmation. In particular, the "front-to-back" pattern of alpha band phases needs to be studied with imaging techniques that have the required high spatial and temporal resolution. Furthermore the model predicts that microstates consist of clusters of phase leading and phase lagging regions, and that specific brain regions may have characteristic patterns of phase relations with other regions. In future studies the directed phase lag index and the model could be used to address further questions concerning the relation between the magnitude of phase differences, conduction delays and speed of information processing, notably in white matter disorders; the influence of local brain lesions on brain network organization and the relation between brain network topology and the efficiency of stimulus processing.

References

Alstott, J., Breakspear, M., Hagmann, P., Cammoun, L., Sporns, O., 2009. Modeling the impact of lesions in the human brain. PLoS Comput. Biol. 5, e1000408.
Bassett, D.S., Bullmore, E.T., 2009. Human brain networks in health and disease. Curr. Opin. Neurol. 22, 340–347.
Boulanger, J.M., Deacon, C., Lécuyer, D., Gosselin, S., Reiher, J., 2006. Triphasic waves versus nonconvulsive status epilepticus: EEG distinction. Can. J. Neurol. Sci. 33, 175–180.
Bullmore, E., Sporns, O., 2009. Complex brain networks: graph theoretical analysis of structural and functional systems. Nat. Rev. Neurosci. 10, 186–198.
Burns, A., 2004. Fourier-, Hilbert- and wavelet-based signal analysis: are they really different approaches? J. Neurosci. Methods 137, 321–332.
Coombes, S., 2010. Large-scale neural dynamics: simple and complex. Neuroimage 52, 731–739.
de Haan, W., Mott, K., van Straaten, E.C.W., van der Flier, W., Scheltens, P., Stam, C.J., in press. Activity Dependent Degeneration Explains Hub Vulnerability in Alzheimer's Disease. PloS Comput. Biol.
Deco, G., Jirsa, V.K., Robinson, P.A., Breakspear, M., Friston, K., 2008. The dynamic brain: from spiking neurons to neural masses and cortical fields. PLoS Comput. Biol. 4, e1000092.

Deco, G., Jirsa, V.K., McIntosh, A.R., 2011. Emerging concepts for the dynamical organization of resting-state activity in the brain. Nat. Rev. Neurosci. 12, 43–56.
Fries, P., 2005. A mechanism for cognitive dynamics: neuronal communication through neuronal coherence. Trends Cogn. Sci. 9, 474–480.
Gong, G., He, Y., Concha, L., Lebel, C., Gross, D.W., Evans, A.C., Beaulieu, C., 2009. Mapping anatomical connectivity patterns of human cerebral cortex using in vivo diffusion tensor imaging tractography. Cereb. Cortex 19, 524–536.
Gourévitch, B., Bouquin-Jeannès, R.L., Faucon, G., 2006. Linear and nonlinear causality between signals: methods, examples and neurophysiological applications. Biol. Cybern. 95, 349–369.
Hafkemeijer, A., van der Grond, J., Rombouts, S.A., 2012. Imaging the default mode network in aging and dementia. Biochim. Biophys. Acta 1822, 431–441.
Hillebrand, A., Barnes, G.R., Bosboom, J.L., Berendse, H.W., Stam, C.J., 2012. Frequency-dependent functional connectivity within resting-state networks: an atlas-based MEG beamformer solution. Neuroimage 59, 3909–3921.
Honey, C.J., Sporns, O., 2008. Dynamical consequences of lesions in cortical networks. Hum. Brain Mapp. 29, 802–809.
Honey, C.J., Kötter, R., Breakspear, M., Sporns, O., 2007. Network structure of cerebral cortex shapes functional connectivity on multiple time scales. Proc. Natl. Acad. Sci. U.S.A. 104, 10240–10245.
Honey, C.J., Sporns, O., Cammoun, L., Gigandet, X., Thiran, J.P., Meuli, R., Hagmann, P., 2009. Predicting human resting-state functional connectivity from structural connectivity. Proc. Natl. Acad. Sci. U.S.A. 106, 2035–2040.
Kaiser, M., Martin, R., Andras, P., Young, M.P., 2007. Simulation of robustness against lesions of cortical networks. Eur. J. Neurosci. 25, 3185–3192.
Kramer, M.A., Cash, S.S., 2012. Epilepsy as a disorder of cortical network organization. Neuroscientist. http://dx.doi.org/10.1177/1073858411422754 (Epub ahead of print).
Lehmann, D., Faber, P.L., Gianotti, L.R., Kochi, K., Pascual-Marqui, R.D., 2006. Coherence and phase locking in the scalp EEG and between LORETA model sources, and microstates as putative mechanisms of brain temporo-spatial functional organization. J. Physiol. Paris 99, 29–36.
Llinás, R., Ribary, U., 1993. Coherent 40-Hz oscillation characterizes dream state in humans. Proc. Natl. Acad. Sci. U.S.A. 90, 2078–2081.
Lopes da Silva, F.H., Hoeks, A., Smits, A., Zetterberg, L.H., 1974. Model of brain rhythmic activity. Kybernetik 15, 27–37.
Massimini, M., Huber, R., Ferrarelli, F., Hill, S., Tononi, G., 2004. The sleep slow oscillation as a traveling wave. J. Neurosci. 24, 6862–6870.
Musso, F., Brinkmeyer, J., Mobascher, A., Warbrick, T., Winterer, G., 2010. Spontaneous brain activity and EEG microstates. A novel EEG/fMRI analysis approach to explore resting-state networks. Neuroimage 52, 1149–1161.
Palva, S., Kulashekhar, S., Hämäläinen, M., Palva, J.M., 2011. Localization of cortical phase and amplitude dynamics during visual working memory encoding and retention. J. Neurosci. 31, 5013–5025.
Ponten, S.C., Daffertshofer, A., Hillebrand, A., Stam, C.J., 2010. The relationship between structural and functional connectivity: graph theoretical analysis of an EEG neural mass model. Neuroimage 52, 985–994.
Rosenblum, M.G., Pikovsky, A.S., Kurths, J., 1996. Phase synchronization of chaotic oscillators. Phys. Rev. Lett. 76, 1804–1807.
Rubinov, M., Bassett, D.S., 2011. Emerging evidence of connectomic abnormalities in schizophrenia. J. Neurosci. 31, 6263–6265.
Rubinov, M., Sporns, O., van Leeuwen, C., Breakspear, M., 2009. Symbiotic relationship between brain structure and dynamics. BMC Neurosci. 10, 55.
Siri, B., Quoy, M., Delord, B., Cessac, B., Berry, H., 2007. Effects of Hebbian learning on the dynamics and structure of random networks with inhibitory and excitatory neurons. J. Physiol. Paris 101, 136–148.
Soddu, A., Vanhaudenhuyse, A., Demertzi, A., Bruno, M.A., Tshibanda, L., Di, H., Mélanie, B., Papa, M., Laureys, S., Noirhomme, Q., 2011. Resting state activity in patients with disorders of consciousness. Funct. Neurol. 26, 37–43.
Spiegler, A., Knösche, T.R., Schwab, K., Haueisen, J., Atay, F.M., 2011. Modeling brain resonance phenomena using a neural mass model. PLoS Comput. Biol. 7, e1002298.
Sporns, O., Zwi, J.D., 2004. The small world of the cerebral cortex. Neuroinformatics 2, 145–162.
Stam, C.J., 2010. Characterization of anatomical and functional connectivity in the brain: a complex networks perspective. Int. J. Psychophysiol. 77, 186–194.
Stam, C.J., Reijneveld, J.C., 2007. Graph theoretical analysis of complex networks in the brain. Nonlinear Biomed. Phys. 1, 3.
Stam, C.J., van Straaten, E.C.W., 2012. The organization of physiological brain networks. Clin. Neurophysiol. 123, 1067–1087. http://dx.doi.org/10.1016/j.clinph.2012.01.011.
Stam, C.J., Pijn, J.P.M., Suffczynski, P., Lopes da Silva, F.H., 1999. Dynamics of the human alpha rhythm: evidence for non-linearity? Clin. Neurophysiol. 110, 1801–1813.
Stam, C.J., Nolte, G., Daffertshofer, A., 2007. Phase lag index: assessment of functional connectivity from multi channel EEG and MEG with diminished bias from common sources. Hum. Brain Mapp. 28, 1178–1193.
Stam, C.J., Hillebrand, A., Wang, H., Van Mieghem, P., 2010. Emergence of modular structure in a large-scale brain network with interactions between dynamics and connectivity. Front. Comput. Neurosci. 24 (4) (pii: 133).
Stephan, K.E., Roebroeck, A., 2012. A short history of causal modeling of fMRI data. Neuroimage. http://dx.doi.org/10.1016/j.neuroimage.2012.01.034 (Epub ahead of print).
Suffczynski, P., Wendling, F., Bellanger, J.-J., Lopes da Silva, F.H., 2006. Some insights into computational models of (patho)physiological brain activity. Proc. IEEE 94, 784–804.
Tzourio-Mazoyer, N., Landeau, B., Papathanassiou, D., Crivello, F., Etard, O., Delcroix, N., Mazoyer, B., Joliot, M., 2002. Automated anatomical labeling of activations in SPM using a macroscopic anatomical parcellation of the MNI MRI single-subject brain. Neuroimage 15, 273–289.
Ursino, M., Zavaglia, M., Astolfi, L., Babiloni, F., 2007. Use of a neural mass model for the analysis of effective connectivity among cortical regions based on high resolution EEG recordings. Biol. Cybern. 96, 351–365.
van den Heuvel, M.P., Hulshoff Pol, H.E., 2010. Exploring the brain network: a review on resting-state fMRI functional connectivity. Eur. Neuropsychopharmacol. 20, 519–534.
van den Heuvel, M.P., Sporns, O., 2011. Rich-club organization of the human connectome. J. Neurosci. 31, 15775–15786.
Wang, S.J., Hilgetag, C.C., Zhou, C., 2011. Sustained activity in hierarchical modular neural networks: self-organized criticality and oscillations. Front. Comput. Neurosci. 5, 30.
Xie, T., He, Y., 2011. Mapping the Alzheimer's brain with connectomics. Front. Psychiatry 2, 77.
Zetterberg, L.H., Kristiansson, L., Mossberg, K., 1978. Performance of a model for a local Neuron population. Biol. Cybern. 31, 15–26.